Polymer Chemistry

PAPER

View Article Online
View Journal | View Issue



Cite this: *Polym. Chem.*, 2015, **6**, 4167

# Phase separation and self-assembly of cyclic amphiphilic block copolymers with a main-chain liquid crystalline segment†

Satoshi Honda,‡ Maito Koga, Masatoshi Tokita,* Takuya Yamamoto* and Yasuyuki Tezuka*

Received 9th March 2015,
Accepted 26th April 2015

DOI: 10.1039/c5py00346f

www.rsc.org/polymers

A series of linear and cyclized amphiphilic block copolymers consisting of poly(acrylic acid) ($AA_m$) and main-chain liquid crystalline (LC) poly(3-methylpentamethylene-4,4′-bibenzoate) ($BB_n$) segments were newly synthesized. Solid state morphology was investigated by X-ray scattering. Linear $AA_{21}BB_9AA_{21}$, cyclic $AA_{33}BB_{10}$, and cyclic $AA_{51}BB_{18}$ formed lamellar microdomains, where the $BB_n$ segment of cyclic $AA_{51}BB_{18}$ formed a smectic CA phase. On the other hand, cylinder-type microdomains were formed by linear $AA_{44}BB_9AA_{44}$ and cyclic $AA_{100}BB_9$. These amphiphilic block copolymers were self-assembled in water to form vesicles or cylindrical micelles, depending on the polymer concentration of the initial THF solution. The response of these nanostructures against an electric field demonstrated that the vesicles formed from linear $AA_{25}BB_{14}AA_{25}$ and cyclic $AA_{51}BB_{18}$ turned into substantially larger aggregates, likely due to the reorganization of the LC segment in the bilayer.

## Introduction

Liquid crystalline (LC) polymers are arguably one of the most widely studied polymeric materials for applications such as indicating and recording elements. Owing to the rigidity and dielectric anisotropy of the polymer chain, LC polymeric materials exhibit a sensitive response to an electric or magnetic field by the macroscopic alignment of microdomains.[1] Side-chain LC segments were sometimes block copolymerized with incompatible segments to exhibit combinational functions with phase separation.[2] Moreover, living polymerization techniques allowed to synthesize amphiphilic block copolymers with a side-chain LC segment as the hydrophobe.[3,4] Notably, an amphiphile having a polyacrylate derivative segment appending an azobenzene functionality exhibited light-responsive order–disorder of the vesicular bilayer *via* the *cis–trans* conformational change.[4] However, no studies have reported the self-assembly of an amphiphilic block copolymer with a main-chain LC segment and electric or magnetic field-responsive properties to take full advantage of the LC segment.

In the meantime, cyclization of a series of linear compounds with biphenyl functionalities resulted in different LC transition behaviors despite no significant changes in the chemical structure or molecular weight.[5] Furthermore, we previously reported that self-assembly of a cyclized amphiphilic block copolymer resulted in a drastic enhancement of *topology effects* on the thermal and salt stability of the micelles in comparison with those from the linear prepolymers.[6] Therefore, the self-assembly of a cyclic amphiphilic block copolymer involving a LC segment was expected to lead to the enhancement of topology effects on the LC functionalities of the aggregate including a response to an electric or magnetic field.

Here linear amphiphilic triblock copolymers and their cyclized counterparts were synthesized composed of hydrophilic poly(acrylic acid) ($AA_m$) segments and a hydrophobic poly(3-methylpentamethylene-4,4′-bibenzoate) ($BB_n$) segment, one of the most studied main-chain LC polymers.[7–9] Their solid state morphologies and phase transition behaviors in the LC segments of these amphiphilic block copolymers were studied. Furthermore, self-assembly in water was performed to give vesicles and cylindrical micelles depending on the conditions. Interestingly, the respective nanostructures responded to an electric field to transform to larger vesicles and an agglomerated network structure.

*Department of Organic and Polymeric Materials, Tokyo Institute of Technology, O-okayama, Meguro-ku, Tokyo 152-8552, Japan.*
*E-mail: mtokita@polymer.titech.ac.jp, yamamoto.t.ay@m.titech.ac.jp, ytezuka@o.cc.titech.ac.jp*

†Electronic supplementary information (ESI) available: SEC traces, $^1$H NMR spectra, DSC thermograms, a supporting table, WAXD intensity profiles, TEM images, a photograph for the experimental setup to apply an electric field. See DOI: 10.1039/c5py00346f

‡Present Address: Department of Industrial Chemistry, Faculty of Engineering, Tokyo University of Science, 12-1 Ichigaya-Funagawara, Shinjuku, Tokyo 162-0826, Japan.

# Experimental

## Materials

All commercial reagents were used as received unless otherwise noted. THF (>99.0%, Kanto Chemical Co., Inc.) was distilled over a Na wire. *tert*-Butyl acrylate (*t*BA) was passed through an alumina column to remove the inhibitor and bubbled with dry nitrogen for 30 min. Hydroxy-terminated $BB_n$ (molecular weight by $^1$H NMR, $M_n$ = 1700) was synthesized according to the literature.[9] A bromo-terminated bifunctional polystyrene macroinitiator was synthesized by atom transfer radical polymerization (ATRP) of styrene from benzal bromide.[10] Poly(acrylic acid)–polystyrene–poly(acrylic acid) ($AA_{134}St_{34}AA_{134}$) was prepared by ATRP of *t*BA from a polystyrene macroinitiator and subsequent hydrolysis of the *tert*-butyl groups according to the reported procedure.[11]

## Synthesis of $BB_n$ macroinitiators

$BB_n$ macroinitiators having bromoisobutyryl groups at the chain ends were synthesized through esterification of hydroxy-terminated $BB_n$ with 2-bromoisobutyryl bromide according to a modified procedure in the literature.[9] Thus, into an anhydrous $CH_2Cl_2$ solution (100 mL) of hydroxy-terminated $BB_n$ (10.0 g, 5.7 mmol, $M_n$ = 1700) and triethylamine (10.4 mL, 75 mmol), 2-bromoisobutyryl bromide (7.6 mL, 62 mmol) was added dropwise at 0 °C. The solution was allowed to warm to room temperature and stirred for 19 h under a nitrogen atmosphere. The reaction mixture was filtered and poured into water (100 mL), and the aqueous phase was extracted by three portions of $CH_2Cl_2$ (100 mL). The combined organic extract was evaporated to dryness under reduced pressure, and the residue was reprecipitated into MeOH to give a $BB_n$ macroinitiator (7.0 g, 2.5 mmol, $M_n$ = 2800) in 43% yield. $^1$H NMR (300 MHz, $CDCl_3$) $\delta$: 1.02–1.15 (m, –$CH_2CH(CH_3)CH_2$–), 1.60–2.00 (m, –$CH_2CH(CH_3)CH_2$–, –$OC(=O)C(CH_3)_2Br$), 4.26 (m, –$CH_2CH_2OC(=O)C(CH_3)_2Br$), 4.36–4.51 (m, –$CH_2CH_2OC$-(=O)Ar–), 7.51–7.65 (m, Ar*H meta* to –$CO_2$–), 8.00–8.12 (m, Ar*H ortho* to –$CO_2$–).

The obtained $BB_n$ macroinitiator was fractionated by preparative size exclusion chromatography (SEC) with THF as an eluent at a flow rate of 14 mL min$^{-1}$. The SEC trace of the fractionated $BB_9$ macroinitiator ($M_n$ = 3400) showed a narrow polydispersity index (PDI = 1.16) but a multimodal peak (peak molecular weight by SEC calibrated with polystyrene standards, $M_p$ = 3800, 3200, 2700, and 2200, Fig. S1a†). The intervals of the multimodal peak corresponded to the $BB_n$ monomer unit ($M$ = 324.37). The $BB_9$ macroinitiator was used for the synthesis of linear $tBA_{21}BB_9tBA_{21}$ and linear $tBA_{50}BB_8tBA_{50}$. A $BB_{14}$ macroinitiator ($M_n$ = 4900, $M_p$ = 7300, PDI = 1.13) was also obtained by SEC fractionation and used for the synthesis of linear $tBA_{27}BB_{18}tBA_{27}$.

## Block copolymerization and allylation

The SEC-fractionated $BB_9$ macroinitiator (458 mg, 0.13 mmol, $M_n$ = 3400), CuBr (36 mg, 0.25 mmol), *t*BA (5.0 mL, 34 mmol), toluene (5.0 mL) were added to a test tube, and the mixture was degassed by three freeze–pump–thaw cycles. The suspension was stirred at 120 °C, and *N*,*N*,*N*′,*N*″,*N*″-pentamethyldiethylenetriamine, PMDETA, (53 μL, 0.25 mmol) was added. The resulting suspension was stirred at 120 °C for 15 min. The reaction mixture was quenched in liquid nitrogen and allowed to warm to room temperature. The remaining monomer was removed under reduced pressure, and allyltributylstannane (0.84 mL, 2.7 mmol) and toluene (5 mL) were added to the residue. The resulting suspension was degassed by three freeze–pump–thaw cycles and stirred at 110 °C for 17 h under vacuum. The reaction mixture was precipitated into cold *n*-hexane, and the solid obtained was filtered through a plug of alumina using $CHCl_3$ as an eluent. The crude product was fractionated by preparative SEC with $CHCl_3$ as an eluent at a flow rate of 3.5 mL min$^{-1}$ and reprecipitated in *n*-hexane to allow isolation of linear $tBA_{21}BB_9tBA_{21}$ (558 mg) in 49% yield. $M_n$(NMR) = 2600–2800–2600, $M_p$ = 10 800, PDI = 1.16. $^1$H NMR (300 MHz, $CDCl_3$) $\delta$: 0.98–1.14 (m, –$CH_2CH(CH_3)CH_2$–), 1.17–2.00 (m, –$CH_2CH(CH_3)CH_2$–, –$OC(=O)C(CH_3)_2$–, –$CH_2CH(CO_2tBu)$–, –$CO_2C(CH_3)_3$, –$CH_2CH=CH_2$), 2.11–2.32 (m, –$CH_2CH(CO_2tBu)$–), 4.10 (m, 4H, –$CH_2CH_2OC(=O)C(CH_3)_2$–), 4.32–4.50 (m, –$CH_2CH_2OC(=O)Ar$–), 4.94–5.07 (m, 4H, –$CH_2CH=CH_2$), 5.68 (m, 2H, –$CH_2CH=CH_2$), 7.49–7.64 (m, Ar*H meta* to –$CO_2$–), 7.98–8.11 (m, Ar*H ortho* to –$CO_2$–).

Likewise, linear $tBA_{27}BB_{18}tBA_{27}$ and linear $tBA_{50}BB_8tBA_{50}$ were synthesized from the $BB_{14}$ and $BB_9$ macroinitiators, respectively. After block copolymerization and allylation, each reaction mixture was precipitated into cold MeOH. The solid obtained was filtered through a plug of alumina using $CHCl_3$ as an eluent to allow the isolation of linear $tBA_{27}BB_{18}tBA_{27}$ and linear $tBA_{50}BB_8tBA_{50}$.

## Metathesis polymer cyclization (MPC)

The second-generation Hoveyda–Grubbs catalyst (92 mg, 0.15 mmol) was added to a toluene solution (800 mL) of linear $tBA_{21}BB_9tBA_{21}$ (200 mg, 24 μmol), and the resulting solution was stirred at 80 °C for 40 h. Ethyl vinyl ether (10 mL) was added to the reaction mixture to quench the catalyst, and the color of the solution immediately changed from brown–green to dark brown. The resulting suspension was stirred for 10 min at 80 °C. After cooling to room temperature, the reaction mixture was concentrated under reduced pressure and filtered through a plug of alumina using $CHCl_3$ as an eluent. The crude product was fractionated by preparative SEC with $CHCl_3$ as an eluent at a flow rate of 3.5 mL min$^{-1}$ to allow the isolation of cyclic $tBA_{31}BB_{10}$ (140 mg) in 78% yield. $M_n$(NMR) = 4000–3300, $M_p$ = 9200, PDI = 1.24. $^1$H NMR (300 MHz, $CDCl_3$) $\delta$: 0.97–1.15 (m, –$CH_2CH(CH_3)CH_2$–), 1.18–2.00 (m, –$CH_2CH(CH_3)CH_2$–, –$OC(=O)C(CH_3)_2$–, –$CH_2CH(CO_2tBu)$–, –$CO_2C(CH_3)_3$, –$CH_2CH=CHCH_2$–), 2.10–2.32 (m, –$CH_2CH(CO_2tBu)$–), 4.10 (m, 4H, –$CH_2CH_2OC(=O)C(CH_3)_2$–), 4.34–4.50 (m, –$CH_2CH_2OC(=O)Ar$–), 5.30 (m, 2H, –$CH_2CH=CHCH_2$–), 7.46–7.64 (m, Ar*H meta* to –$CO_2$–), 7.96–8.11 (m, Ar*H ortho* to –$CO_2$–).

Likewise, cyclic $tBA_{54}BB_{16}$ and cyclic $tBA_{91}BB_8$ were synthesized.

 

### Hydrolysis of linear $t$BA$_m$BB$_n$$t$BA$_m$ and cyclic $t$BA$_{2m}$BB$_n$

Linear $t$BA$_{21}$BB$_9$$t$BA$_{21}$ (50 mg, 5.9 μmol) was dissolved in $CH_2Cl_2$ (10 mL), and trifluoroacetic acid (TFA, 1.9 mL, 25 mmol) was added. The mixture was stirred at room temperature for 14 h under a nitrogen atmosphere. The reaction mixture was concentrated under reduced pressure and precipitated into $CHCl_3$ to allow the isolation of linear AA$_{21}$BB$_9$AA$_{21}$ (35 mg) in 92% yield. $M_n$(NMR) = 1500–3000–1500, $^1$H NMR (300 MHz, $CF_3COOD$) $\delta$: 0.98–1.41 (m, –$CH_2CH(CH_3)CH_2$–), 1.47–2.39 (m, –$CH_2CH(CH_3)CH_2$–, –OC(=O)C($CH_3$)$_2$–, –$CH_2CH(CO_2H)$–, –$CH_2CH{=}CH_2$), 2.50–2.99 (m, –$CH_2CH(CO_2H)$–), 4.22 (m, –$CH_2CH_2OC(=O)C(CH_3)_2$–), 4.33–4.70 (m, –$CH_2CH_2OC(=O)$Ar–), 4.98–5.13 (m, 4H, –$CH_2CH{=}CH_2$), 5.67 (m, 2H, –$CH_2CH{=}CH_2$), 7.36–7.67 (m, Ar*H meta* to –$CO_2$–), 7.86–8.34 (m, Ar*H ortho* to –$CO_2$–).

The hydrolysis of cyclic $t$BA$_{31}$BB$_{10}$ was carried out in the same procedure to give cyclic AA$_{33}$BB$_{10}$ in 85% yield. $M_n$(NMR) = 2400–3400, $^1$H NMR (300 MHz, $CF_3COOD$) $\delta$: 0.94–1.43 (m, –$CH_2CH(CH_3)CH_2$–), 1.48–2.30 (m, –$CH_2CH(CH_3)CH_2$–, –OC(=O)C($CH_3$)$_2$–, –$CH_2CH(CO_2H)$–, –$CH_2CH{=}CHCH_2$–), 2.59–2.85 (m, –$CH_2CH(CO_2H)$–), 4.22 (m, –$CH_2CH_2OC(=O)C(CH_3)_2$–), 4.39–4.65 (m, –$CH_2CH_2OC(=O)$Ar–), 5.48 (m, 2H, –$CH_2CH{=}CHCH_2$–), 7.30–7.63 (m, Ar*H meta* to –$CO_2$–), 7.80–8.09 (m, Ar*H ortho* to –$CO_2$–).

Likewise, linear AA$_{25}$BB$_{14}$AA$_{25}$, cyclic AA$_{51}$BB$_{18}$, linear AA$_{44}$BB$_9$AA$_{44}$, and cyclic AA$_{100}$BB$_9$ were synthesized.

### NMR measurements

$^1$H NMR spectra were recorded at room temperature on a JEOL JNM-AL300 spectrometer operating at 300 MHz. $CDCl_3$ or $CF_3COOD$ was used as a solvent, and chemical shifts were reported relative to the signal of the residual proton of the deuterated solvent.

### SEC measurements

SEC measurements were performed at 40 °C on a HPLC system equipped with a Tosoh CCPS pump, a Tosoh TSK G3000HXL column, and a Tosoh RI 8020 refractive index detector. THF was used as an eluent at a flow rate of 1.0 mL min$^{-1}$. Linear polystyrene standards were used for calibration, and the $M_p$ values were reported as polystyrene equivalents.

### SEC fractionation

SEC fractionation was performed on a JAI LC-908 recycling preparative HPLC system equipped with JAIGEL-2H and JAIGEL-3H columns using $CHCl_3$ as an eluent at a flow rate of 3.5 mL min$^{-1}$ or a JAI LC-9204 recycling preparative HPLC system equipped with two of JAIGEL-2H-40, JAIGEL-3H-40, and JAIGEL-4H-40 columns using THF as an eluent at a flow rate of 14 mL min$^{-1}$.

### X-Ray measurements

Wide-angle X-ray diffraction (WAXD) patterns were measured by a Bruker D8 DISCOVER equipped with a Vantec-500 detector using Cu Kα radiation. The synchrotron radiation (SR)-SAXS measurement was performed at a BL-10C beamline in Photon Factory, Tsukuba, Japan, equipped with a PILATUS3 2M. The X-ray wavelength ($\lambda$) was 0.1488 nm, and the camera length was 2 m. The scattering intensity was plotted against the scattering vector $q = 4\pi \sin\theta/\lambda$. For the preparation of a specimen, an amphiphilic block copolymer cast from a THF solution was heated at 170 °C and then cooled to ambient temperature at a rate of 1 °C min$^{-1}$.

### DSC measurements

Differential scanning calorimetry (DSC) was performed using a PerkinElmer Pyris 1 DSC calorimeter equipped with an Intracooler II under a flow of dry nitrogen. The same specimen preparation method for the X-ray measurements was used.

### Self-assembly

Distilled water (1.0 mL) was slowly added to a vigorously stirred THF solution of linear AA$_m$BB$_n$AA$_m$ or cyclic AA$_{2m}$BB$_n$ (either $c_0$ = 1.0 mg mL$^{-1}$, 1.0 mL or $c_0$ = 10 mg mL$^{-1}$, 0.10 mL, where $c_0$ indicates the polymer concentration of the initial THF solution). THF was removed under reduced pressure, and the resulting suspension was diluted with distilled water to a total volume of 1.0 mL to form a 1.0 mg mL$^{-1}$ aqueous suspension of linear AA$_m$BB$_n$AA$_m$ or cyclic AA$_{2m}$BB$_n$. On the other hand, distilled water (1.0 mL) was added to AA$_{134}$St$_{34}$AA$_{134}$ (10 mg), and the mixture was sonicated. The resulting suspension was diluted with distilled water to a total volume of 10 mL to form a 1.0 mg mL$^{-1}$ aqueous suspension of AA$_{134}$St$_{34}$AA$_{134}$.

### TEM observations

A carbon-coated Formvar film supported by a Cu grid (200 mesh) was plasma glow discharged for 60 s to form a hydrophilic surface. An aqueous suspension (10 μL) of linear AA$_m$BB$_n$AA$_m$, cyclic AA$_{2m}$BB$_n$, or linear AA$_{134}$St$_{34}$AA$_{134}$ was placed on the film, and the excess suspension was removed using a filter paper. For the TEM images of Fig. 3e and f, the samples on the films were stained. Thus, a TI-blue solution (Nisshin EM) was diluted to 5-fold with water. The diluted solution (10 μL) was placed on a sample-loaded film for 60 s and removed using a filter paper. The sample-loaded films with and without staining were carefully dried under reduced pressure. TEM observations were performed on a Hitachi H-7650 Zero A microscope operating at 60 kV.

## Results and discussion

### Synthesis

Macroinitiators possessing a BB$_n$ functionality were prepared by esterification of hydroxy-terminated BB$_n$ ($M_n$ = 1700) with 2-bromoisobutyryl bromide as reported (Scheme 1a).[9] The quantitative conversion of the hydroxyl groups into bromoisobutyryl groups was confirmed by the replacement of the $^1$H NMR signal of the hydroxyl-adjacent methylene protons at 3.73 ppm ("g" in Fig. S2a†) by the ester neighboring methylene protons at 4.26 ppm ("g" in Fig. S2b†). The product was fractio-

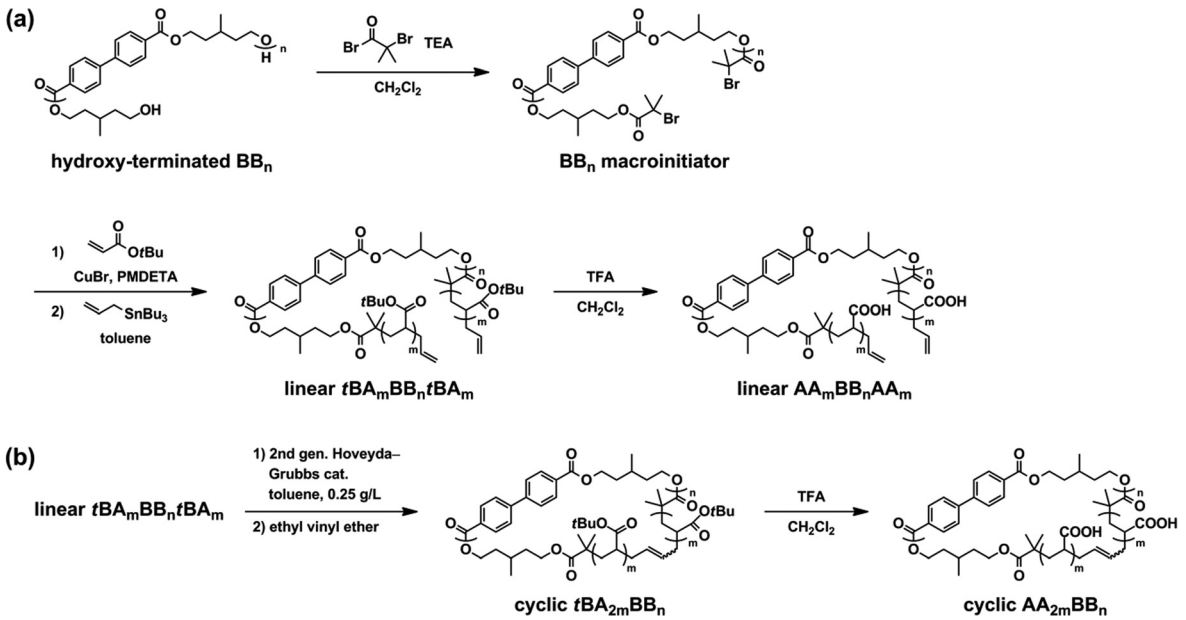


**Scheme 1** Synthesis of (a) linear $AA_mBB_nAA_m$ from hydroxy-terminated $BB_n$ and (b) cyclic $AA_{2m}BB_n$ from linear $tBA_mBB_ntBA_m$.

nated by SEC to give $BB_9$ ($M_n$ = 3400, $M_p$ = 3800, 3200, 2700, and 2200, PDI = 1.16 in Fig. S1a†) and $BB_{14}$ ($M_n$ = 4900, $M_p$ = 7300, PDI = 1.13) macroinitiators. The intervals of the multimodal peak of the $BB_9$ macroinitiator corresponded to the $BB_n$ monomer unit ($M$ = 324.37).

Allyl-telechelic block copolymers were prepared through ATRP of *t*BA from the $BB_n$ macroinitiators in the presence of CuBr and PMDETA followed by allylation of the terminal bromides with allyltributylstannane (Scheme 1a). The effective end-capping reaction was confirmed by the $^1$H NMR signals "m" at 5.68 ppm and "n" at 4.94–5.07 ppm for allyl-terminated linear $tBA_{21}BB_9tBA_{21}$ (Fig. S3a†). In addition, the signals from the two phenylene groups in the $BB_n$ units at 7.98–8.11 ppm for "e" and 7.49–7.64 ppm for "f" and the large signal due to the *tert*-butyl protons at 1.42 ppm for "k" were observed. SEC traces of a $BB_9$ macroinitiator ($M_p$ = 3800, 3200, 2700, and 2200, PDI = 1.16 in Fig. S1a†) and linear $tBA_{21}BB_9tBA_{21}$ ($M_p$ = 10 800, PDI = 1.16 in Fig. S1b†) were compared to show the shift toward the higher molecular weight region with retaining narrow polydispersity, which was indicative of living polymerization. Moreover, the molecular weight of $tBA_m$ segments increased along with the polymerization time (Table 1).

Allyl-telechelic $tBA_mBB_ntBA_m$ was subjected to the metathesis polymer cyclization (MPC) process under the dilution (0.25 g $L^{-1}$) in the presence of the second-generation Hoveyda–Grubbs catalyst.[6,12] The $^1$H NMR spectra of the product from linear $tBA_{21}BB_9tBA_{21}$ showed the signals of the inner olefinic group at 5.30 ppm for both *cis* and *trans* isomers ("m" in Fig. S3c†), completely replacing those from the terminal allyl groups of the prepolymer ("m" and "n" in Fig. S3a†). In addition, the other signals were essentially unaffected through MPC, indicating that no side reactions occurred in the present

**Table 1** Properties of the *t*Bu-protected and deprotected linear and cyclic block copolymers

| *t*Bu-protected block copolymer | | | | | | Deprotected block copolymer[a] | |
|---|---|---|---|---|---|---|---|
| Formula | ATRP time (min) | Cyclization yield | $M_n$ [b] | $M_p$ [c] | PDI[c] | Formula | $M_n$ [b] |
| Linear $tBA_{21}BB_9tBA_{21}$ | 15 | | 2600–2800–2600 | 10 800 | 1.16 | Linear $AA_{21}BB_9AA_{21}$ | 1500–3000–1500 |
| Cyclic $tBA_{31}BB_{10}$ [d] | | 70% | 4000–3300 | 9200 | 1.24 | Cyclic $AA_{33}BB_{10}$ | 2400–3400 |
| Linear $tBA_{27}BB_{18}tBA_{27}$ | 30 | | 3500–5700–3500 | 11 000 | 1.33 | Linear $AA_{25}BB_{14}AA_{25}$ | 1800–4700–1800 |
| Cyclic $tBA_{54}BB_{16}$ [d] | | 38% | 6900–5100 | 6100 | 1.28 | Cyclic $AA_{51}BB_{18}$ | 3700–5900 |
| Linear $tBA_{50}BB_8tBA_{50}$ | 60 | | 6300–2700–6300 | 18 700 | 1.16 | Linear $AA_{44}BB_9AA_{44}$ | 3200–2900–3200 |
| Cyclic $tBA_{91}BB_8$ [d] | | 74% | 11 700–2500 | 17 500 | 1.17 | Cyclic $AA_{100}BB_9$ | 7200–2900 |

[a] $M_p$ or PDI was not measured due to the insolubility of the AA segments in a solvent for SEC. [b] Molecular weights of the $BB_n$, $tBA_m$, and $AA_m$ segments, and thus their numbers of repeating units, were calculated by the peak areas of "a", "j", and "j", respectively, with respect to "g" in the $^1$H NMR spectra (Fig. S3). [c] $M_p$ and PDI were determined using calibration with polystyrene standards. [d] Cyclic $tBA_{31}BB_{10}$, $tBA_{54}BB_{16}$, and $tBA_{91}BB_8$ were synthesized from linear $tBA_{21}BB_9tBA_{21}$, $tBA_{27}BB_{18}tBA_{27}$, and $tBA_{50}BB_8tBA_{50}$, respectively.

 

reaction system. The molecular weights of the prepolymer and the product determined by $^1$H NMR ($M_n$), and thus their formulae (linear $t$BA$_m$BB$_n t$BA$_m$ and cyclic $t$BA$_{2m}$BB$_n$), were somewhat inconsistent with each other due to the purification process to remove intermolecularly coupled products (Table 1).

SEC for cyclic $t$BA$_{31}$BB$_{10}$ showed a unimodal peak in the absence of a noticeable shoulder at the higher molecular weight region after fractionation by preparative SEC ($M_p$ = 9200 in Fig. S1c†). The results of MPC with linear $t$BA$_{27}$BB$_{18}t$BA$_{27}$ and linear $t$BA$_{50}$BB$_8t$BA$_{50}$ are also summarized in Table 1. While the linear precursors with a relatively short BB$_n$ segment (linear $t$BA$_{21}$BB$_9t$BA$_{21}$ and linear $t$BA$_{50}$BB$_8t$BA$_{50}$) showed high yields (≥70%), that of linear $t$BA$_{27}$BB$_{18}t$BA$_{27}$ was comparably low (38%). This was likely caused by the suppressed intramolecular metathesis of the latter having the longer rigid BB$_n$ segment. Nevertheless, the present cyclization process is applicable for a linear $t$BA$_m$BB$_n t$BA$_m$ precursor with a rather high molecular weight (~15 000 for linear $t$BA$_{50}$BB$_8t$BA$_{50}$) with the appropriate length of the BB$_n$ segment.

The $t$BA$_m$ segments were hydrolyzed by trifluoroacetic acid (TFA) to give poly(acrylic acid), AA$_m$, segments in the acid form, forming linear AA$_m$BB$_n$AA$_m$ and cyclic AA$_{2m}$BB$_n$ amphiphilic block copolymers (Scheme 1). As reported elsewhere, a *tert*-butyl ester group is easily deprotectable by the addition of TFA without causing a side reaction.[13] The $^1$H NMR spectra of the products, linear AA$_{21}$BB$_9$AA$_{21}$ (Fig. S3b†) and cyclic AA$_{33}$BB$_{10}$ (Fig. S3d†), showed the disappearance of the signal of the *tert*-butyl protons at 1.42 ppm ("k" in Fig. S3a and S3c†). Moreover, the signals of the allyl groups of linear $t$BA$_{21}$BB$_9t$BA$_{21}$ ("m" at 5.68 ppm and "n" at 4.94–5.07 ppm in Fig. S3a†) and the inner olefinic group of cyclic $t$BA$_{31}$BB$_{10}$ ("m" at 5.30 ppm in Fig. S3c†) as well as the other protons were unaffected through hydrolysis. Likewise, a series of linear AA$_m$BB$_n$AA$_m$ and cyclic AA$_{2m}$BB$_n$ with different molecular weights were synthesized and characterized (Table 1). Also, in this synthetic process, $M_n$ and the formulae of the copolymers shifted due to purification.

### Solid state morphology

The phase separation of these linear and cyclic amphiphilic block copolymers in the solid state was studied. Linear AA$_{21}$BB$_9$AA$_{21}$, cyclic AA$_{33}$BB$_{10}$, and cyclic AA$_{51}$BB$_{18}$ segregated each segment to form lamellar microdomains which display SAXS profiles including maxima at scattering vectors $q$ at integer ratios (Fig. 1). Effects of macrocyclization on the lamellar morphology can be recognized by comparing the SAXS profile of cyclic AA$_{33}$BB$_{10}$ with the linear AA$_{21}$BB$_9$AA$_{21}$ counterpart. The scattering peaks of the linear copolymer are broader than that for the cyclic counterpart, suggesting that the lamellae periodicity was less ordered for the linear copolymer. While the lamellar spacings ($d_{100}$) were comparable to each other (linear AA$_{21}$BB$_9$AA$_{21}$, 9.3 nm; cyclic AA$_{33}$BB$_{10}$, 9.2 nm), the LC lamella thickness estimated from the SAXS peak intensity ratios was larger for the cyclic copolymer (linear AA$_{21}$BB$_9$AA$_{21}$, 3.3 nm; cyclic AA$_{33}$BB$_{10}$, 5.9 nm) as shown in Table 2. Though the macrocyclization decreased the $M_n$ of the AA$_m$ segment to increase the BB$_n$ volume fraction by a factor of $\phi_{v,\ BB_n,\ cyclic}/\phi_{v,\ BB_n,\ linear}$ = 0.57/0.48 = 1.2, the BB$_n$ lamellar thickness increases by a factor of 5.9 nm/3.3 nm = 1.8, which was remarkably larger than that expected from the difference in $\phi_{v,\ BB_n}$. Thus the macrocyclization by connecting the AA$_m$ segments at both chain ends decreases the AA$_m$ lamella thickness and increases the middle BB$_n$ segment lamella thickness to maintain the lamellar spacing constant.

Here we note that the BB$_n$ segments in both copolymers might form an ordered phase. Both copolymers exhibited DSC thermograms including two steps at around 55 °C and 100 °C attributed to the glass transition of BB$_n$ and AA$_m$ segments, respectively, and an endothermic peak at around 140 °C in the heating process (Fig. S4a and S4b†). The ordered phase seems to be different from the smectic CA phase formed by the BB$_n$ homopolymer because it exhibited higher $T_g$ and lower $T_i$ and smaller $\Delta H_i$ than that of the smectic CA (SmCA) phase ($T_g$ = 30 °C, $T_i$ = 150 °C, and $\Delta H_i$ = 3.8 kJ mol$^{-1}$).[8] Moreover both copolymers did not display the layer reflection characteristic of the SmCA phase with a $d$-spacing of 1.63 nm in the WAXD intensity profiles (Fig. S5†). In contrast, the BB$_n$ segment of cyclic AA$_{51}$BB$_{18}$ formed the SmCA phase displaying the layer reflection with $d$ = 1.63 nm in the WAXD pattern though $T_i$ = 111 °C and $\Delta H_i$ = 2.33 kJ mol$^{-1}$ (Fig. S4c, Table S1†) were smaller than that of the homopolyester and was accommodated in 7.1 nm thick lamellae (Table 2). The average contour length of the BB$_{18}$ was 29.3 nm determined by a layer spacing of 1.63 nm multiplied by the number of BB$_n$ units. Assuming that the BB$_n$ segments are most extended perpendicular to the lamellar interface, the BB$_n$ segment folds at every 4.4 units on average to be accommodated in the 7.1 nm thick lamellae. The average number of folding was 3.1 ((29.3 nm/7.1 nm) − 1). The odd number of folding may be in accord with the cyclic topology of the copolymer (Fig. 2c). The lamellar microdomain structures thus elucidated are depicted in Fig. 2a–c.

The pair of linear AA$_{44}$BB$_9$AA$_{44}$ and cyclic AA$_{100}$BB$_9$ formed cylinder-type microdomains displaying scattering peaks at $q$ with ratios of $1:4^{0.5}:9^{0.5}$ (Fig. 1d and e). It should be noted that the $3^{0.5}$ peak is missing. This suggests that its position may correspond to the position of the first zero of the form factor. In the SAXS profiles, the square of the calculated form factor for a cylinder of 3.9 nm in radius is presented with solid lines. The first zero arises at around $q$ = 1.0 nm$^{-1}$, which corresponds to the position of the $3^{0.5}$ peak as found in Fig. 1d and e. The distance between two adjacent cylinder centers was estimated to be 12.7 and 12.4 nm for the linear and cyclic copolymers, respectively (Fig. 2d and e). From the volume fractions of each segment, the BB$_n$ segments were assumed to be accommodated within the cylinders. Both copolymers did not exhibit the endothermic peak (Fig. S4d and S4e†), and the layer reflection was ascribed to be the smectic phase formed by the BB-5 (3-Me) homopolyester (Fig. 1d and e), suggesting that the BB$_n$ segment is amorphous. Here the macrocyclization by connecting the AA$_m$ segments at both chain ends can decrease the volume fraction of the AA$_m$ segments immersing the BB$_n$-segment cylinders. Though the BB$_n$ volume fraction calculated

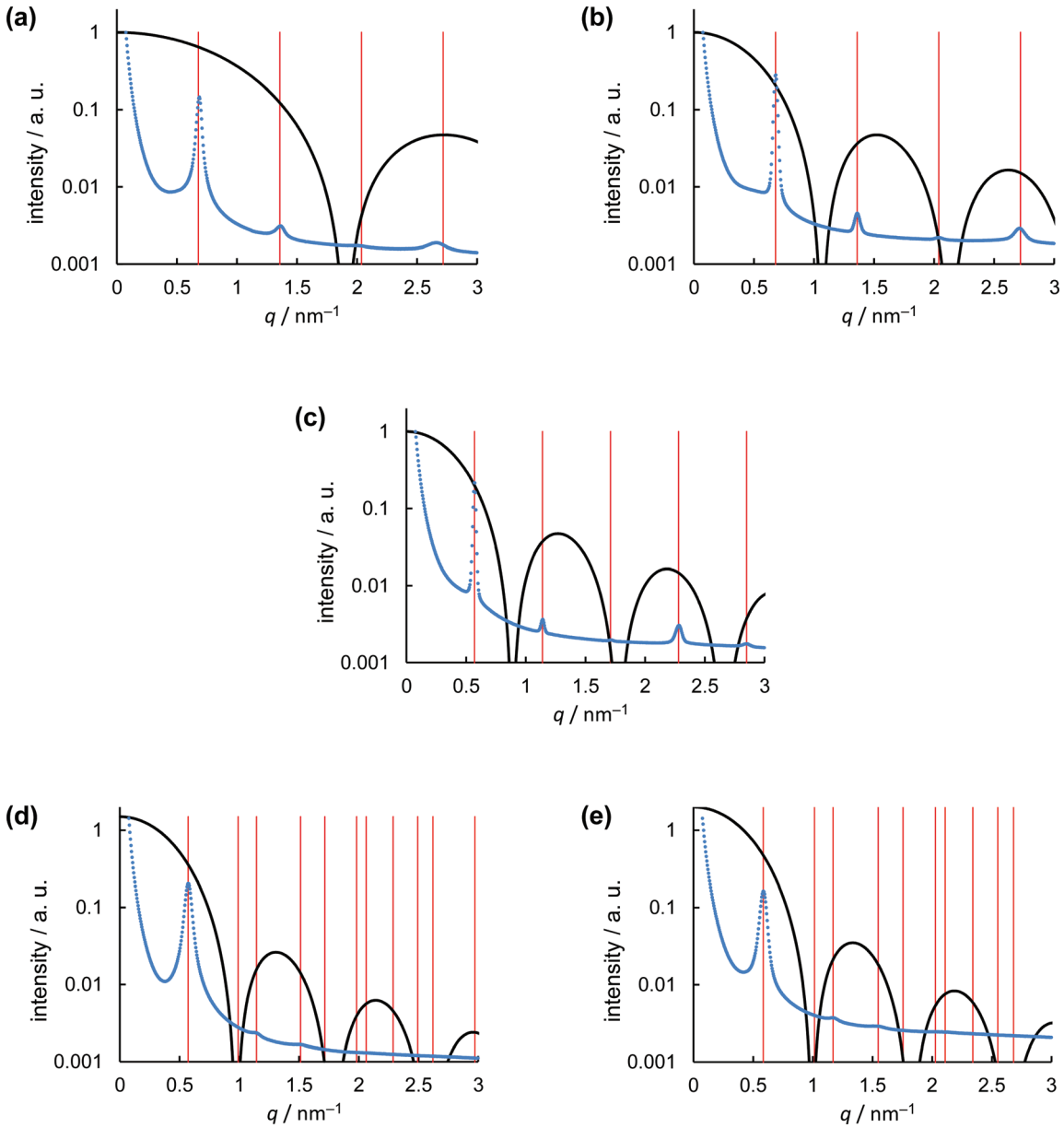


**Fig. 1** SAXS intensity profile (blue dots) measured for (a) linear $AA_{21}BB_9AA_{21}$, (b) cyclic $AA_{33}BB_{10}$, (c) cyclic $AA_{51}BB_{18}$, (d) linear $AA_{44}BB_9AA_{44}$, and (e) cyclic $AA_{100}BB_9$. Black curves and red lines are the square of the form factor and the lattice factor, respectively, calculated for (a–c) two-phase lamellar microdomains and (d) and (e) cylinder microdomains with the parameters shown in Table 2.

from the $M_n$ of each segment was 0.30 and 0.27 for the linear and cyclic copolymers, respectively, that calculated from the dimensions of the cylinder microdomain was 0.35 for both copolymers (see Table 2).

### Self-assembly in water

Some of the linear and cyclic amphiphilic block copolymers were self-assembled in water to determine the topology effects on discrete structures. Self-assembly of linear $AA_{21}BB_9AA_{21}$, linear $AA_{25}BB_{14}AA_{25}$, cyclic $AA_{33}BB_{10}$, and cyclic $AA_{51}BB_{18}$ was carried out by evaporating a good solvent from a mixture of the good solvent and water that contained an amphiphilic block copolymer,[14] and the resulting nanostructure was observed by transmission electron microscopy (TEM). Thus, distilled water (1.0 mL) was slowly added to a vigorously stirred THF solution of a copolymer (1.0 mg $mL^{-1}$, 1.0 mL). THF was removed under reduced pressure, and distilled water was added to a total volume of 1.0 mL to form an aqueous suspension of the copolymer (1.0 mg $mL^{-1}$). The TEM images of suspensions containing each of self-assembled linear $AA_{21}BB_9AA_{21}$ and cyclic $AA_{33}BB_{10}$ showed a cylindrical micellar morphology with approximately 20–30 nm in width (Fig. S6a and S6b†). No significant difference between linear $AA_{21}BB_9AA_{21}$ and cyclic $AA_{33}BB_{10}$ was observed despite the

 

Table 2 Solid morphology of linear $AA_{21}BB_9AA_{21}$, cyclic $AA_{33}BB_{10}$, cyclic $AA_{51}BB_{18}$, linear $AA_{44}BB_9AA_{44}$, and cyclic $AA_{100}BB_9$ determined by SAXS

| | Structure | $d_{100}$ (nm) | $\phi_{v,\,BB_n}$ | Lamellar thickness or cylinder radius (nm) |
|---|---|---|---|---|
| Linear $AA_{21}BB_9AA_{21}$ | Lamellar | 9.3 | 0.48[a] | 4.5[a] |
| | | | 0.35[b] | 3.3[b] |
| Cyclic $AA_{33}BB_{10}$ | Lamellar | 9.2 | 0.57[a] | 5.3[a] |
| | | | 0.64[b] | 5.9[b] |
| Cyclic $AA_{51}BB_{18}$ | Lamellar with LC phases | 11.0 | 0.60[a] | 6.6[a] |
| | | | 0.64[b] | 7.1[b] |
| Linear $AA_{44}BB_9AA_{44}$ | Cylinder | 11.0 | 0.30[a] | 3.6[a] |
| | | | 0.35[b] | 3.9[b] |
| Cyclic $AA_{100}BB_9$ | Cylinder | 10.7 | 0.27[a] | 3.4[a] |
| | | | 0.35[b] | 3.9[b] |

[a] Based on the molecular weights and density of each segment. [b] Based on the structural factors estimated from SAXS intensity.

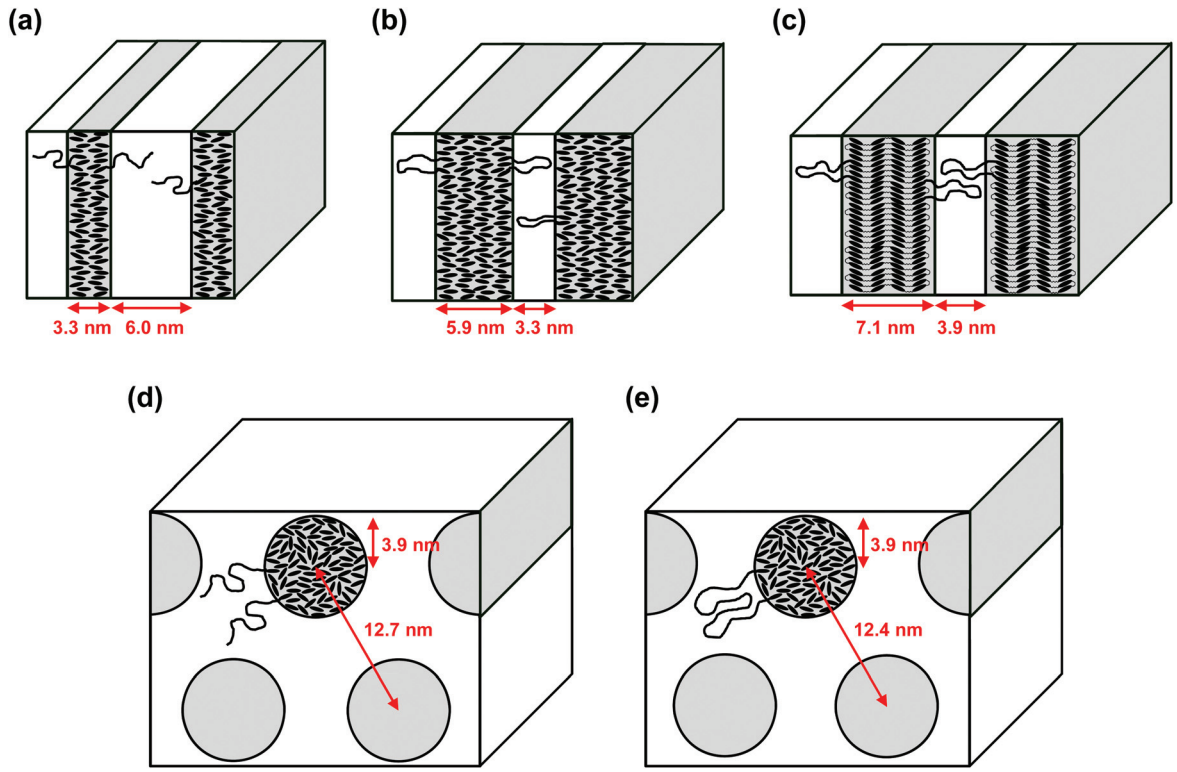


Fig. 2 Phase separation models of (a) linear $AA_{21}BB_9AA_{21}$, (b) cyclic $AA_{33}BB_{10}$, (c) cyclic $AA_{51}BB_{18}$, (d) linear $AA_{44}BB_9AA_{44}$, and (e) cyclic $AA_{100}BB_9$.

changes in the topology and the molecular weight of the $AA_m$ segments. On the other hand, the structure formed by linear $AA_{25}BB_{14}AA_{25}$ (Fig. 3a) was quite uniform, while that observed for cyclized $AA_{51}BB_{18}$ was much less continuous (Fig. 3b). According to the critical packing parameter (CPP) theory,[15] the hydrophobic/hydrophilic balance of an amphiphilic block copolymer determines the morphology of the self-assembly.[15,16] The concurrent formation of discrete micelles indicates that cyclic $AA_{51}BB_{18}$ had a significantly smaller CPP than linear $AA_{25}BB_{14}AA_{25}$. Although the molecular weight fraction of the $BB_n$ segment is larger for cyclic $AA_{51}BB_{18}$ (5900/(3700 + 5900) = 0.61) than linear $AA_{25}BB_{14}AA_{25}$ (4700/(1800 + 4700 + 1800) = 0.57) as shown in Table 1, the cyclic topology was expected to restrict the conformational degree of freedom of the $BB_n$ segment compared to that of the linear counterpart, resulting in a smaller CPP. Models for the cylindrical micelles are depicted in Fig. S7.†

The dependence of the self-assembled structure on the polymer concentration of the initial THF solution ($c_0$) was subsequently investigated. Generally, self-assembly is strongly influenced by the diffusion process of a poor solvent into a good solvent that solvates the less soluble segment.[17] There-

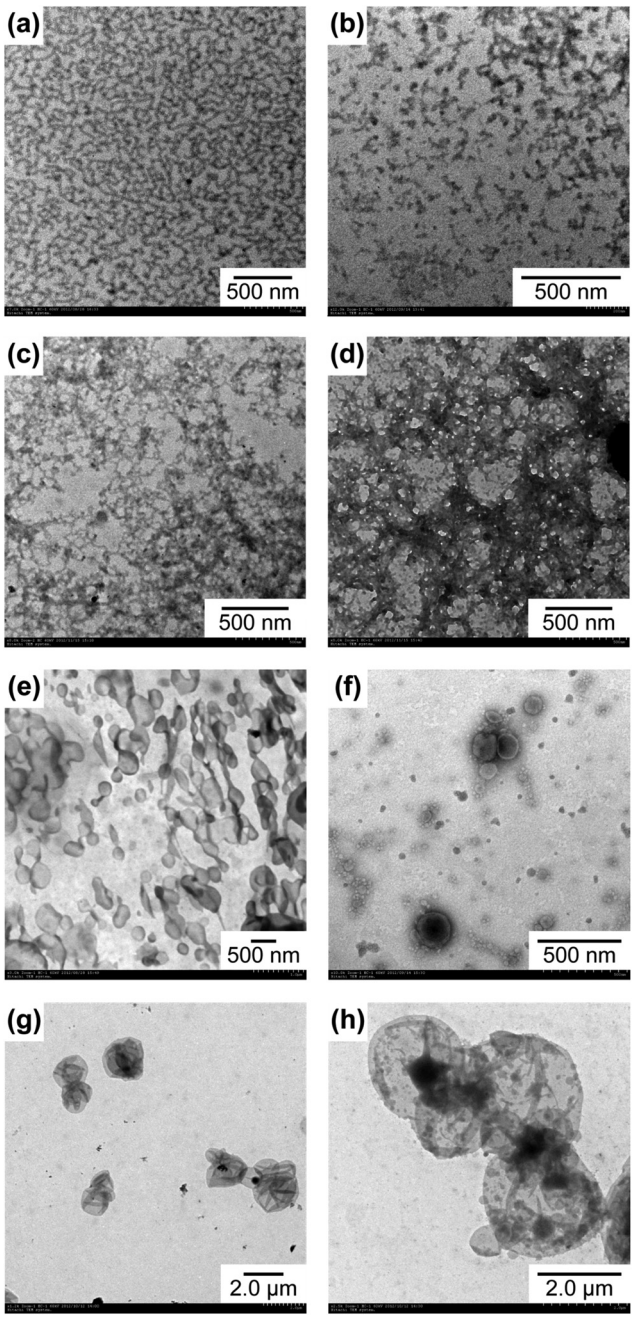


**Fig. 3** TEM images of self-assembled structures from linear $AA_{25}BB_{14}AA_{25}$ and cyclic $AA_{51}BB_{18}$ using an initial THF solution with a polymer concentration ($c_0$) of 1.0 and 10 mg mL$^{-1}$ before and after applying an electric field ($E$) of 1.5 V mm$^{-1}$ for 2 min. (a) Linear, $c_0$ = 1.0 mg mL$^{-1}$, before $E$. (b) Cyclic, $c_0$ = 1.0 mg mL$^{-1}$, before $E$. (c) Linear, $c_0$ = 1.0 mg mL$^{-1}$, after $E$. (d) Cyclic, $c_0$ = 1.0 mg mL$^{-1}$, after $E$. (e) Linear, $c_0$ = 10 mg mL$^{-1}$, before $E$, stained with TI-blue. (f) Cyclic, $c_0$ = 10 mg mL$^{-1}$, before $E$, stained with TI-blue. (g) Linear, $c_0$ = 10 mg mL$^{-1}$, after $E$. (h) Cyclic, $c_0$ = 10 mg mL$^{-1}$, after $E$.

fore, to investigate the possible formation of other structures by controlling the diffusion kinetics, $c_0$ was increased to 10 mg mL$^{-1}$. For self-assembly of the linear $AA_{21}BB_9AA_{21}$ (Fig. S6c†) and the corresponding cyclic $AA_{33}BB_{10}$ (Fig. S6d†), the predominant morphology was still cylindrical micelles. Although discrete spherical micelles were observed only for linear $AA_{21}BB_9AA_{21}$, the effect of $c_0$ seemed rather small for these copolymers. In sharp contrast, the morphology of the aggregates from linear $AA_{25}BB_{14}AA_{25}$ and the corresponding cyclic $AA_{51}BB_{18}$ were notably changed to vesicles. The size of the vesicles formed from cyclic $AA_{51}BB_{18}$ was *ca.* 20–200 nm in diameter with a certain degree of size distribution (Fig. 3f). On the other hand, the vesicles from linear $AA_{25}BB_{14}AA_{25}$ were larger (mostly *ca.* 200 nm–500 nm in diameter, Fig. 3e), and those as large as 2 μm were also found. TI-blue, a staining agent, was used on these vesicles to show sufficient contrast in the TEM images. Although dynamic light scattering measurements were attempted, the size distributions could not be obtained, likely due to the fact that the exceedingly large distributions did not allow for fitting of the data. Compared to linear $AA_{21}BB_9AA_{21}$ and cyclic $AA_{33}BB_{10}$, linear $AA_{25}BB_{14}AA_{25}$ and cyclic $AA_{51}BB_{18}$ had a relatively longer $BB_n$ segment, which tended to form a bilayer for vesicles. The formation of vesicles from an amphiphile with a longer hydrophobic chain is consistent with the CPP theory[15] as well as previous reports.[17,18]

### Response to an electric field

Although several studies have so far been performed on the self-assembly of an amphiphilic block copolymer having a LC segment to construct discrete structures,[3,4] their electric or magnetic field response, which is the most characteristic property of a LC polymer, has not been reported. To the vesicles and cylindrical micelles obtained from the present linear and cyclic LC copolymers, an electric field was applied to investigate their response. The experimental setup is shown in Fig. S8.† In order to prevent electrolysis of water, the effective minimal strengths of the electric field (1.5 V mm$^{-1}$) and time (2 min) were optimized. The effects on the self-assembled structures were observed by TEM. Interestingly, the vesicles from cyclic $AA_{51}BB_{18}$ became significantly larger by applying an electric field (as large as *ca.* 3 μm in diameter, Fig. 3h). Small vesicles of tens to hundreds of nanometers were also observed at the surface of the micrometer-scale vesicles. Moreover, the bilayer was rather clearly observed even without staining. It was expected that the self-assembled vesicles transformed into the larger vesicles by the fusion of the bilayer through the reorganization of the LC segments in response to the electric field. The reorganization likely gave a thermodynamically more stable, more regulated, and robust bilayer, resulting in the significantly larger aggregate size and the clear appearance in the TEM image. For linear $AA_{25}BB_{14}AA_{25}$, vesicles of 1–2 μm in diameter were observed after applying an electric field (Fig. 3g). No smaller vesicles (200–500 nm) that existed in Fig. 3e were found, suggesting that the small vesicles were re-assembled into the micrometer-scale vesicles. The vesicles from linear $AA_{25}BB_{14}AA_{25}$ and cyclic $AA_{51}BB_{18}$ were rather similar in size after applying an electric field than those self-assembled. These results suggest that the topology, and possibly also the difference in the molecular weight of the $BB_n$ segment caused by purification, play a more significant role

 

during the self-assembly process than the reorganization by an electric field. In the meantime, the cylindrical micelles formed from the respective linear and cyclic copolymers using a $c_0$ of 1.0 mg $mL^{-1}$ became an agglomerated network structure under the same electric field conditions (Fig. 3c and d). The $BB_n$ unit has dielectric anisotropy between the long and short axes of the biphenyl group, and the long axis is aligned parallel to an applied electric field. The isotropic transformation to form the larger vesicles and agglomerated networks was probably caused by the rotation of the structures in the solvent. In accord with the reported transformation of vesicles by the osmotic pressure,[17,19] the details of the present phenomenon are currently under investigation.

Since poly(acrylic acid) is an anionic polymer, the observed electric field response could be caused by the negative surface charge of the nanostructures. To confirm the effect of the $BB_n$ segment on the electric field response, a polystyrene ($St_n$) counterpart, linear $AA_{134}St_{34}AA_{134}$, was used for the electric field-applying experiment. Self-assembly gave a spherical nanostructure with 300 nm or less in diameter with a large size distribution (Fig. S9a†). However, this nanostructure did not show any response to an electric field (Fig. S9b†). Therefore, the electric field response of the vesicles and cylindrical micelles indeed arose from the $BB_n$ segment.

## Conclusions

Series of linear and cyclized amphiphilic block copolymers consisting of hydrophilic $AA_m$ and hydrophobic $BB_n$ segments were synthesized, where $BB_n$ is a typical main-chain LC. The phase separation in the solid state was studied on the basis of the topology and segment lengths of the copolymers. The self-assembly in water led to the formation of vesicles or cylindrical micelles depending on $c_0$. The application of an electric field resulted in the reorganization of the $BB_n$ segment, giving rise to the transformation to micrometer-scale vesicles or an agglomerated network structure. The utilization of the present methodology would widely open the application of voltage-sensing materials. Furthermore, the amphiphilic block copolymers having a main-chain LC segment reported here resemble voltage sensor-containing phosphatase (VSP) for ion channels and transporters.[20,21] Therefore, the dynamic motions upon applying an electric field would mimic the VSP functions of the cell membrane to deliver electric signals.[20]

## Acknowledgements

The authors are grateful to Prof. M. Kakimoto for access to NMR facilities. We thank the Center for Advanced Materials Analysis, Technical Department, Tokyo Institute of Technology for TEM observations. This work was supported by the Grant-in-Aid for JSPS Fellows (249031, S.H.), Mizuho Foundation for the Promotion of Sciences (S.H.), Global COE Program (Education and Research Center for Material Innovation), MEXT, Japan (S.H.), and KAKENHI (26288099 T.Y. and 26310206 Y.T.). The SR-SAXS measurement has been performed under the approval of the Photon Factory Program Advisory Committee (no. 2013G544).

## References

1 A. M. Donald, A. H. Windle and S. Hanna, *Liquid Crystalline Polymers*, Cambridge University Press, Cambridge, U.K., 2nd edn, 2006.
2 (*a*) W. Y. Zheng and P. T. Hammond, *Macromol. Rapid Commun.*, 1996, **17**, 813–824; (*b*) M. Petr, B.-a. Katzman, W. DiNatale and P. T. Hammond, *Macromolecules*, 2013, **46**, 2823–2832.
3 (*a*) C. Osuji, P. J. Ferreira, G. Mao, C. K. Ober, J. B. Vander Sande and E. L. Thomas, *Macromolecules*, 2004, **37**, 9903–9908; (*b*) J. Yang, D. Levy, W. Deng, P. Keller and M. H. Li, *Chem. Commun.*, 2005, 4345–4347; (*c*) H. Yu, A. Shishido, T. Ikeda and T. Iyoda, *Macromol. Rapid Commun.*, 2005, **26**, 1594–1598; (*d*) E. Mabrouk, D. Cuvelier, L.-L. Pontani, B. Xu, D. Levy, P. Keller, F. Brochard-Wyart, P. Nassoy and M.-H. Li, *Soft Matter*, 2009, **5**, 1870–1878.
4 B. Yan, X. Tong, P. Ayotte and Y. Zhao, *Soft Matter*, 2011, **7**, 10001–10009.
5 M. Itoh, M. Tokita, K. Adachi, T. Hayakawa, S. Kang, Y. Tezuka and J. Watanabe, *Liq. Cryst.*, 2009, **36**, 1443–1450.
6 (*a*) S. Honda, T. Yamamoto and Y. Tezuka, *J. Am. Chem. Soc.*, 2010, **132**, 10251–10253; (*b*) S. Honda, T. Yamamoto and Y. Tezuka, *Nat. Commun.*, 2013, **4**, 1574; (*c*) *Topological Polymer Chemistry: Progress of Cyclic Polymers in Syntheses, Properties and Functions*, ed. Y. Tezuka, World Scientific, Singapore, 2013.
7 (*a*) J. Watanabe, M. Hayashi, A. Morita and M. Tokita, *Macromolecules*, 1995, **28**, 8073–8079; (*b*) J. Watanabe, M. Hayashi and M. Tokita, *React. Funct. Polym.*, 1996, **30**, 191–196; (*c*) M. Tokita, K. Osada and J. Watanabe, *Polym. J.*, 1998, **30**, 589–595.
8 (*a*) K. Osada, H. Niwano, M. Tokita, S. Kawauchi and J. Watanabe, *Macromolecules*, 2000, **33**, 7420–7425; (*b*) K. Osada, M. Koike, H. Tagawa, M. Tokita and J. Watanabe, *Macromol. Chem. Phys.*, 2004, **205**, 1051–1057.
9 R. Ishige, T. Ishii, M. Tokita, M. Koga, S. Kang and J. Watanabe, *Macromolecules*, 2011, **44**, 4586–4588.
10 M. Al-Harthi, A. Sardashti, J. B. P. Soares and L. C. Simon, *Polymer*, 2007, **48**, 1954–1961.
11 K. A. Davis and K. Matyjaszewski, *Macromolecules*, 2000, **33**, 4039–4047.
12 Y. Tezuka and R. Komiya, *Macromolecules*, 2002, **35**, 8667–8669.
13 (*a*) S. Abraham, C.-S. Ha and I. Kim, *J. Polym. Sci., Part A: Polym. Chem.*, 2005, **43**, 6367–6378; (*b*) S. Hietala, S. Strandman, P. Jarvi, M. Torkkeli, K. Jankova, S. Hvilsted and H. Tenhu, *Macromolecules*, 2009, **42**, 1726–1732.
14 D. Wang, Z. Peng, X. Liu, Z. Tong, C. Wang and B. Ren, *Eur. Polym. J.*, 2007, **43**, 2799–2808.

15 (*a*) J. N. Israelachvili, D. J. Mitchell and B. W. Ninham, *J. Chem. Soc., Faraday Trans. 2*, 1976, **72**, 1525–1568; (*b*) J. Israelachvili, *Colloids Surf., A*, 1994, **91**, 1–8.

16 (*a*) A. Stein, S. G. Rudisill and N. D. Petkovich, *Chem. Mater.*, 2014, **26**, 259–276; (*b*) S. I. Stupp and L. C. Palmer, *Chem. Mater.*, 2014, **26**, 507–518.

17 K. T. Kim, J. Zhu, S. A. Meeuwissen, J. J. L. M. Cornelissen, D. J. Pochan, R. J. M. Nolte and J. C. M. van Hest, *J. Am. Chem. Soc.*, 2010, **132**, 12522–12524.

18 (*a*) L. Zhang and A. Eisenberg, *J. Am. Chem. Soc.*, 1996, **118**, 3168–3181; (*b*) Y. S. Yu, L. F. Zhang and A. Eisenberg, *Macromolecules*, 1998, **31**, 1144–1154.

19 (*a*) W. Helfrich and R. M. Servuss, *Il Nuovo Cimento D*, 1984, **3**, 137–151; (*b*) D. H. W. Hubert, M. Jung, P. M. Frederik, P. H. H. Bomans, J. Meuldijk and A. L. German, *Langmuir*, 2000, **16**, 8973–8979; (*c*) J. Pencer, G. F. White and F. R. Hallett, *Biophys. J.*, 2001, **81**, 2716–2728; (*d*) P. Saveyn, J. Cocquyt, P. Bomans, P. Frederik, M. De Cuyper and P. Van der Meeren, *Langmuir*, 2007, **23**, 4775–4781; (*e*) H. Yuan, C. Huang and S. Zhang, *Soft Matter*, 2010, **6**, 4571–4579; (*f*) S. A. Meeuwissen, K. T. Kim, Y. Chen, D. J. Pochan and J. C. M. van Hest, *Angew. Chem., Int. Ed.*, 2011, **50**, 7070–7073; (*g*) R. Salva, J.-F. Le Meins, O. Sandre, A. Brûlet, M. Schmutz, P. Guenoun and S. Lecommandoux, *ACS Nano*, 2013, **7**, 9298–9311.

20 Y. Murata, H. Iwasaki, M. Sasaki, K. Inaba and Y. Okamura, *Nature*, 2005, **435**, 1239–1243.

21 M. Sasaki, M. Takagi and Y. Okamura, *Science*, 2006, **312**, 589–592.

 